Frequency optimisation for DC/DC converters in DC-connected offshore wind turbines

Victor Timmers, Agustí Egea-Àlvarez
UNIVERSITY OF STRATHCLYDE
204 George Street, G1 1XW
Glasgow, United Kingdom
victor.timmers@strath.ac.uk

Aris Gkountaras
SIEMENS GAMESA
Beim Strohhause 17-31, 20097
Hamburg, Germany
aris.gkountaras@siemensgamesa.com

ACKNOWLEDGMENT

This work was funded by EPSRC Industrial CASE number EP/T517665/1 and Siemens Gamesa.

***Index Terms*—DC-DC converter, Wind energy, Design optimization, Multi-objective optimization, Power density optimisation.**

***Abstract*—In all-DC wind farms, DC/DC converters connect the low voltage wind turbine output to the high voltage DC array. One potential benefit of using DC/DC converters is that they require a relatively small transformer due to their higher frequency operation. However, there is no consensus as to what this frequency should be. This paper aims to determine the optimal operating frequency for DC/DC converters in 15 MW wind turbines connected to an 80 kV DC array. A multi-objective optimisation is performed taking into account the DC/DC converter volume, weight and losses. Frequencies ranging from 500 Hz to 5 kHz were tested for unidirectional, bidirectional, single-phase and three-phase converters. The optimal frequencies for unidirectional and bidirectional converters were found to be approximately 2 kHz and 1 kHz, respectively.**

I. INTRODUCTION

All-DC wind farms, where both the collection and export systems use DC cables, have been proposed as a method to reduce the levelised cost of offshore wind generation. In traditional wind farms, large 50 Hz transformers are required to step up the voltage, both in the wind turbines and at the farm-level [1]. For offshore wind farms with HVDC export systems, the offshore platform which houses the AC/DC converter and farm-level transformers accounts for some of the largest capital costs of the wind farm [2].

In all-DC wind farms, voltage conversion can be performed through the use of DC/DC converters. Most DC/DC converter designs employ a medium frequency transformer (MFT), operating at constant frequency, to step up the voltage and provide galvanic isolation. The higher frequency allows for a more compact design, saving space and weight. For the farm-level converter, the smaller converter footprint and weight results in a reduction in the offshore platform costs [3]. For the wind turbine converter, a compact DC/DC converter allows the voltage conversion to be performed in the nacelle, avoiding the need for large low voltage cables in the wind turbine tower. However, high operating frequencies can lead to increased switching losses, reducing the overall efficiency of the system. This research focuses on the wind turbine converter, but the methodology could be applied to the farm-level converter as well.

The selection of the converter frequency is an important research question, which has no definitive answer in the literature. Many studies assume a certain frequency with minimal justification, which can range from as little as 500 Hz [4] up to 10 kHz [5]. There is therefore a need for studies to quantify the trade-offs of the DC/DC converter operating frequency.

A small number of studies have attempted to determine suitable operating frequencies for DC wind turbines. In [6], the efficiency and transformer volume of a single-phase dual active bridge (DAB1) converter were calculated for frequencies varying from 500 Hz to 10 kHz. The results showed that for a SiC-based converter, a switching frequency of 2 kHz corresponded with the most efficient operation, whereas switching frequencies of up to 6 kHz provided a 50% volume reduction at minimal efficiency penalty. For a DAB1 using IGBTs, the most efficient switching frequency was found to be 1 kHz, with frequencies up to 3 kHz providing a 40% volume reduction at the cost of a 0.5% efficiency decrease.

In [7], the volume, mass, and power losses of six different converter topologies were calculated for frequencies ranging from 500 Hz to 20 kHz. Two of the tested topologies were unidirectional DC/DC con-

This is a peer-reviewed, accepted author manuscript of the following conference paper: Timmers, V., Egea-Àlvarez, A., & Gkountaras, A. (2023). Frequency optimisation for DC/DC converters in DC-connected offshore wind turbines. In 2023 25th European Conference on Power Electronics and Applications (EPE'23 ECCE Europe) IEEE. https://doi.org/10.23919/EPE23ECCEEurope58414.2023.102645111

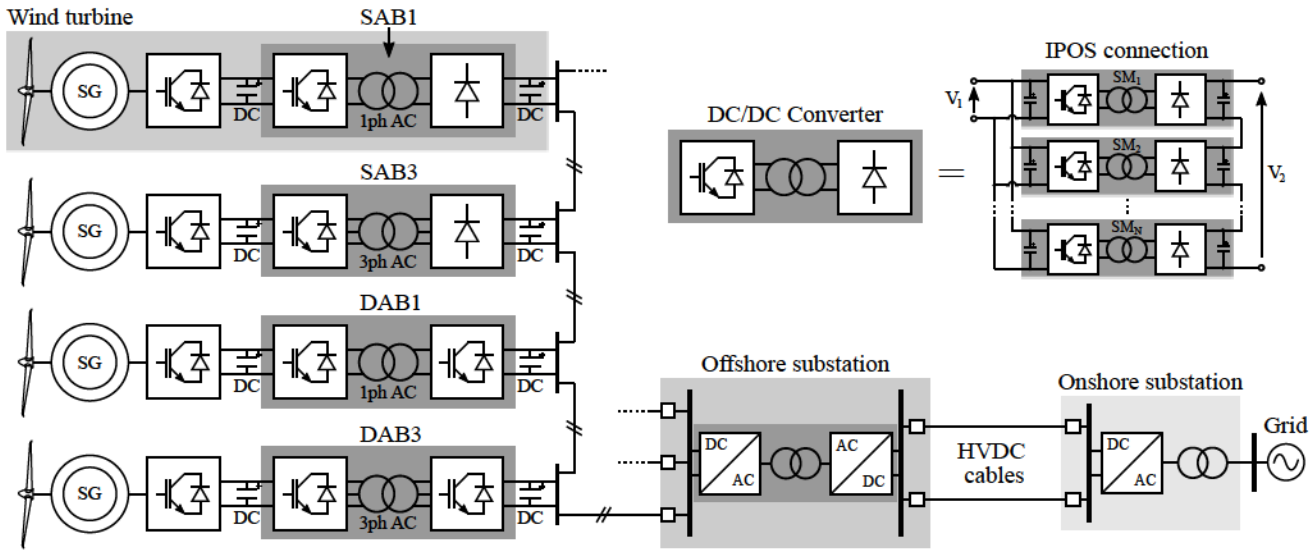

Fig. 1: Considered wind turbine DC/DC converter options in an all-DC wind farm

verters that used a MFT with square wave operation, including a single-phase and three-phase variation. The study found that the losses increased monotonically with frequency, mass decreased with frequency, whereas the lowest volumes were obtained for frequencies ranging from 2 kHz to 3 kHz. The selected frequency for the DC/DC converter was 2.43 kHz.

A key issue with these studies is that they do not make any comparisons between unidirectional and bidirectional converters. Unidirectional converters are expected to provide the most cost-effective solution since they use diodes in the rectifying bridge. However, bidirectional power converters would enable self-start capabilities in case of a black start, since power is required to energise the DC bus and to supply the auxiliary equipment [8]. The additional switches of the bidirectional converter may result in a different optimal operating frequency. There is therefore a need for studies comparing these configurations.

In addition, the rapid development of wind turbines has resulted in the considered wind turbine power and voltage ratings in previous studies to already be outdated. At the same time, previous studies only take into account loss estimates at nominal power output, whereas wind turbines do not continually output this power.

This study aims to fill these research gaps by considering both unidirectional and bidirectional, single-phase and three-phase converters, suited to the latest generation of offshore wind turbines. The power losses for each converter are calculated over the entire operating range to create a more representative efficiency measure.

II. System Configuration

Four wind turbine converter topologies were considered in this research, including the single-phase single active bridge (SAB1), three-phase single active bridge (SAB3), single-phase dual active bridge (DAB1), and three-phase dual active bridge (DAB3). The four converter types and their location in an all-DC wind farm are illustrated in Fig. 1. For a detailed description of the operation of the tested converters, refer to [9]–[11].

Each converter topology contains an active two-level voltage source inverter at the input, followed by an optimised MFT, and a passive or active output bridge for the unidirectional and bidirectional topologies, respectively. The latest generation of wind turbines have ratings of 15 MW [12] and array voltages of 66 kV AC are now standard, with plans for further increases to 132 kV [13]. A DC array voltage of 80 kV is therefore considered in this study [3]. To achieve these ratings, each DC/DC converter cascades multiple individual converter submodules using an input-parallel, output-series (IPOS) connection, as shown in Fig. 1.

The number of IPOS connected submodels was determined based on the voltage and current ratings of the selected semiconductors, with additional redundant modules added to increase the converter reliability, following the methodologies used in [14], [15]. The selected IGBT for the input bridge of all converter topologies is the Infineon FF1800R171P5 [16], due to its standard voltage rating for generator-side converters and its high current rating. For the SAB converters, the output bridge diodes were chosen to be the Infineon D471N [17], which have

TABLE I: Converter parameters

Parameter	Description	Unit	Value
P_1	Converter input power	MW	15
V_2	Converter output voltage	kV	80
N_{SAB1}	Number of submodules for SAB1		17
N_{SAB3}	Number of submodules for SAB3		16
N_{DAB1}	Number of submodules for DAB1		24
N_{DAB3}	Number of submodules for DAB3		22

TABLE II: Material properties for the MFT [14], [20]

Symbol	Property	Unit	Value
B_{sat}	Core magnetic saturation	T	1.17
ρ_c	Core density	kg/m^3	7330
k_c	Core fill factor		0.75
κ	First Steinmetz constant	W/m^3	0.036
α	Second Steinmetz constant		1.64
β	Third Steinmetz constant		2.10
E_{max}	Max. insulation strength	kV/mm	29

the highest available voltage rating. For the output bridge of the DAB converters, the selected IGBT is the Infineon FD250R65KE3-K [18]. For all semiconductors, a typical voltage de-rating factor of 60% was assumed to account for voltage transients. The resulting converter parameters are given in Table I.

III. Size and Weight

The transformer provides the largest contribution to both the volume and weight of the converter [19]. To determine the MFT design for each frequency, an optimisation process is conducted, based on the procedure set out in [20]. The single-phase transformers are considered to be shell type with the low and high voltage windings concentrically wound around the central limb. The three-phase transformers are assumed to be core type with the low and high voltage windings wound concentrically around each of the three limbs. The geometry is illustrated in Fig. 2.

The design procedure starts with the specification of fixed design parameters, such as nominal power, input and output voltages and frequency. In addition, the core and insulation materials are selected, shown in Table II. The transformer windings are assumed to be copper foil in the primary and litz wires in the secondary.

The operating frequency has a direct impact on the transformer design. The required core cross section is calculated using

$$A_{core} = \frac{\lambda_1}{2N_1 B_{max} k_c} \tag{1}$$

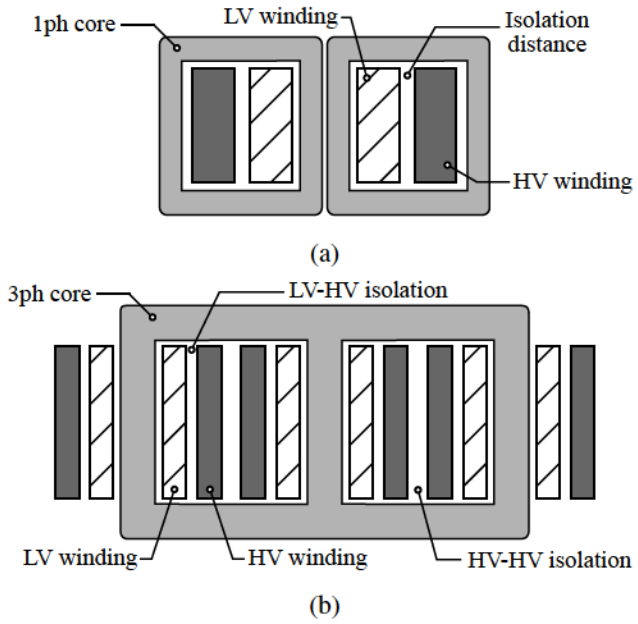

Fig. 2: Medium frequency transformer arrangement, (a) single-phase, (b) three-phase

where N_1 is the number of turns in the primary, B_{max} is the maximum flux density, assumed to be 80% of the core material's saturation flux density, and k_c is the core fill factor. The maximum flux linkage, λ_1, is calculated by integrating the positive half cycle of the magnetising voltage

$$\lambda_1 = \int_0^{T_{pos}} v_p(t)\, dt = \frac{k_\lambda V_1}{f} \tag{2}$$

where k_λ is equal to the maximum duty cycle for the SAB1, $\frac{1}{2}$ for the DAB1, and $\frac{2}{9}$ for the SAB3 and DAB3.

In addition to the core cross section, the required inductance of the system is also inversely proportional to the frequency. The required inductance is incorporated in the transformer in the form of its leakage inductance. The leakage inductance is determined by the transformer geometry and isolation distance between the LV and HV windings, d_{iso}. It can be calculated using [21]

$$L = \mu_0 N_1^2 \left(\frac{\mathrm{MLT}_1 w_1}{3h_1} + \frac{\mathrm{MLT}_2 w_2}{3h_2} + \frac{2\mathrm{MLT}_{iso} d_{iso}}{h_1 + h_2} \right) \tag{3}$$

where μ_0 is the permeability of free space, MLT is the mean length of a turn, w is the coil width, and h is the coil height. The subscripts 1, 2 and iso, indicate the LV winding, HV winding, and inter-winding space, respectively.

Many of these parameters are not fixed and will depend on the specific transformer geometry. Therefore, to obtain an optimal design, the calculations are performed for a range of free parameters. These include the

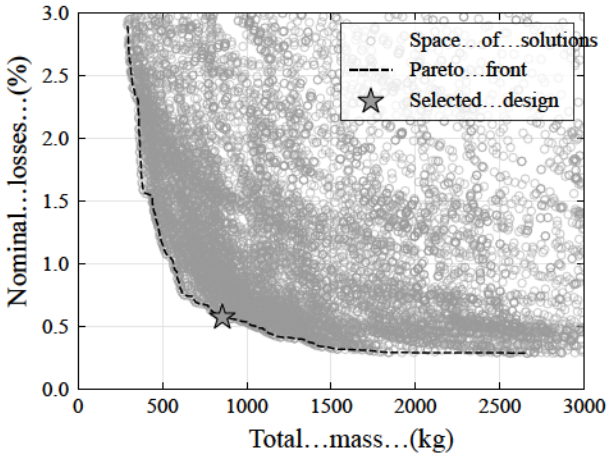

Fig. 3: Multi-objective optimisation of the MFT for the DAB1 converter operating at 1 kHz

number of parallel layers in the primary and secondary windings, the number of turns per layer in the primary, the number of core stacks, the current density of the primary and secondary windings, and the ratio of limb width to thickness. This results in tens of thousands of possible transformer designs, which are each evaluated in terms of volume, weight and losses.

From this large space of solutions, a Pareto-optimal front is calculated, and the selected design for comparison can be determined by minimising the objective function

$$f_{obj} = \left(\frac{P_{tr}}{P_{tr,min}}\right)^{x} + \frac{M_{tot}}{M_{tot,min}} + \frac{V_{tot}}{V_{tot,min}} \tag{4}$$

where P_{tr} are the transformer losses, M_{tot} is the total mass of the transformer, and V_{tot} is the total volume of the transformer. The exponent x has a value of 2 or 3 for the single-phase and three-phase MFTs, respectively. The subscript min indicates those designs which have the minimum value for one of these parameters. An example of this process is shown for one converter topology and one frequency in Fig. 3.

IV. Efficiency

The efficiency calculations include an assessment of the transformer core and winding losses, as well as the switching and conduction losses of the input and output bridge semiconductors. This section details the equations and methodology used in these calculations.

A. Transformer losses

The AC current waveform in the transformer windings will determine the copper losses. Each converter is simulated in PLECS for operating points ranging from 0.1 pu to 1.0 pu. The winding currents are extracted and the harmonic orders are calculated using the Fast Fourier Transform (FFT). The DC winding resistance for each winding is calculated using

$$R_{dc} = \frac{\rho_{Cu} N \mathrm{MLT}}{A_{Cu}} \tag{5}$$

where ρ_{Cu} is the resistivity of copper, and A_{Cu} is the cross-sectional area of the copper.

To account for the skin effect, the ratio of AC to DC resistance at a given harmonic frequency f_h is calculated using the equations [22]

$$K_{ac} = \frac{1}{2} y M_y + (2m-1)^2 D_y \tag{6}$$

where

$$y = \frac{w_c}{\delta} \quad ; \quad \delta = \sqrt{\frac{\rho_{Cu}}{\pi \mu_0 \mu_r f_h}} \tag{7}$$

$$M_y = \frac{\sinh(y) + \sin(y)}{\cosh(y) - \cos(y)} \tag{8}$$

$$D_y = \frac{\sinh(y) - \sin(y)}{\cosh(y) + \cos(y)} \tag{9}$$

where w_c is the conductor width, m is the number of parallel layers in the coil, and μ_r is the relative permeability of copper.

The copper winding losses can then be calculated by summing the losses for each harmonic component

$$P_{Cu} = \sum_h I_h^2 K_{ac,h} R_{dc} \tag{10}$$

where I_h is the magnitude of the current with harmonic order h, and $K_{ac,h}$ is the ratio of AC to DC resistance at the frequency of harmonic order h.

Similarly, to determine the iron losses, the transformer magnetisation voltage and associated flux density change were calculated for each operating point. The Improved Generalised Steinmetz Equation (IGSE) can then be used to calculate the iron losses per unit volume. The IGSE is given by [23]

$$P_{core} = \frac{1}{T} \int_0^T k_i \left|\frac{dB}{dt}\right|^{\alpha} (\Delta B)^{\beta-\alpha} dt \tag{11}$$

where B is the instantaneous magnetic flux density, ΔB is the peak-to-peak magnetic flux density, and k_i is calculated using

$$k_i = \frac{k}{(2\pi)^{\alpha-1} \int_0^{2\pi} |\cos\theta|^{\alpha} 2^{\beta-\alpha} d\theta} \tag{12}$$

where k, α, and β are the Steinmetz parameters of the iron core material.

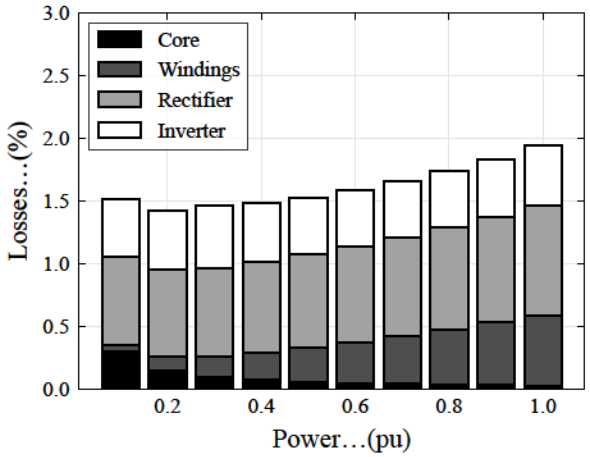

Fig. 4: Converter losses for the DAB1 operating at 1 kHz

B. Semiconductor losses

The semiconductor losses consist of the conduction losses and switching losses and were simulated in PLECS. The conduction losses are calculated using

$$P_{cond} = \frac{1}{T}\int_0^T v_{on} i_{on} dt \tag{13}$$

where P_{cond} are the conduction losses, v_{on} is the on-state forward voltage drop of the device, and i_{on} is the current through the device. The on-state voltage drop is determined through linear interpolation of a look-up table [24], based on the publicly available datasheet [16].

The semiconductor switching losses are calculated using

$$P_{sw} = \frac{1}{T}\sum(E_{on} + E_{off} + E_{rr}) \tag{14}$$

where E_{on} are the turn-on losses, E_{off} are the turn-off losses and E_{rr} are the reverse recovery losses, which are calculated in PLECS using a 3D lookup table, given by

$$E = f(v_{block}, i_{on}, \theta) \tag{15}$$

where E is the relevant energy loss during switching, v_{block} is the semiconductor blocking voltage, i_{on} is the on-state current and θ is the temperature, all determined either pre- or post-switching [24].

An example of the transformer and semiconductor loss calculation across the operating range is shown in Fig. 4 for one converter topology at one frequency. It can be seen that the semiconductor losses account for the largest proportion of losses. This is the case for all tested converters. Of the remaining transformer losses, the winding losses account for the majority of losses, except at very low power outputs.

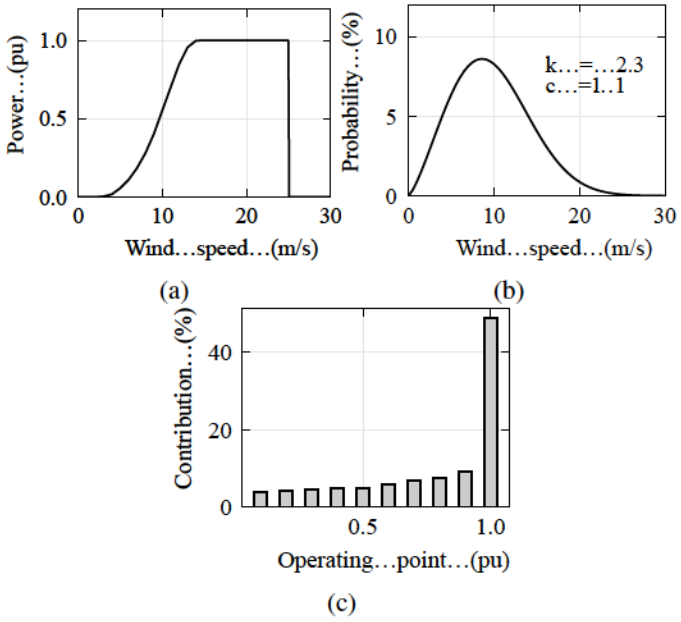

Fig. 5: Representative losses calculation: (a) wind turbine power curve, (b) Weibull probability distribution of the wind speed, (c) relative contribution of each operating point

C. Representative losses

Since the converter does not operate at nominal power continuously, a representative measure of the losses needs to be calculated. To do this, first the converter losses are evaluated for operating points ranging from 0.1 pu to 1.0 pu using the methodology described in the previous subsections. This data can then be transformed into a representative measure based on the total losses the converter is expected to experience under typical wind conditions.

The power output of the wind turbine at each wind speed is calculated using a generic power curve, based on [3]. This is shown in Fig. 5a. This curve allows the required wind speed for each operating point to be extracted.

A Weibull distribution of the wind speed is assumed with a typical shape parameter k of 2.3 and a scale parameter c of 11, as shown in Fig. 5b. Using this curve, the number of hours at each operating point is determined.

The total annual losses are derived using the combination of loss data and the annual hours for each operating point. Finally, the representative loss figure is given by the ratio of the annual losses to the annual power production. The relative contribution of each operating point is illustrated in Fig. 5c.

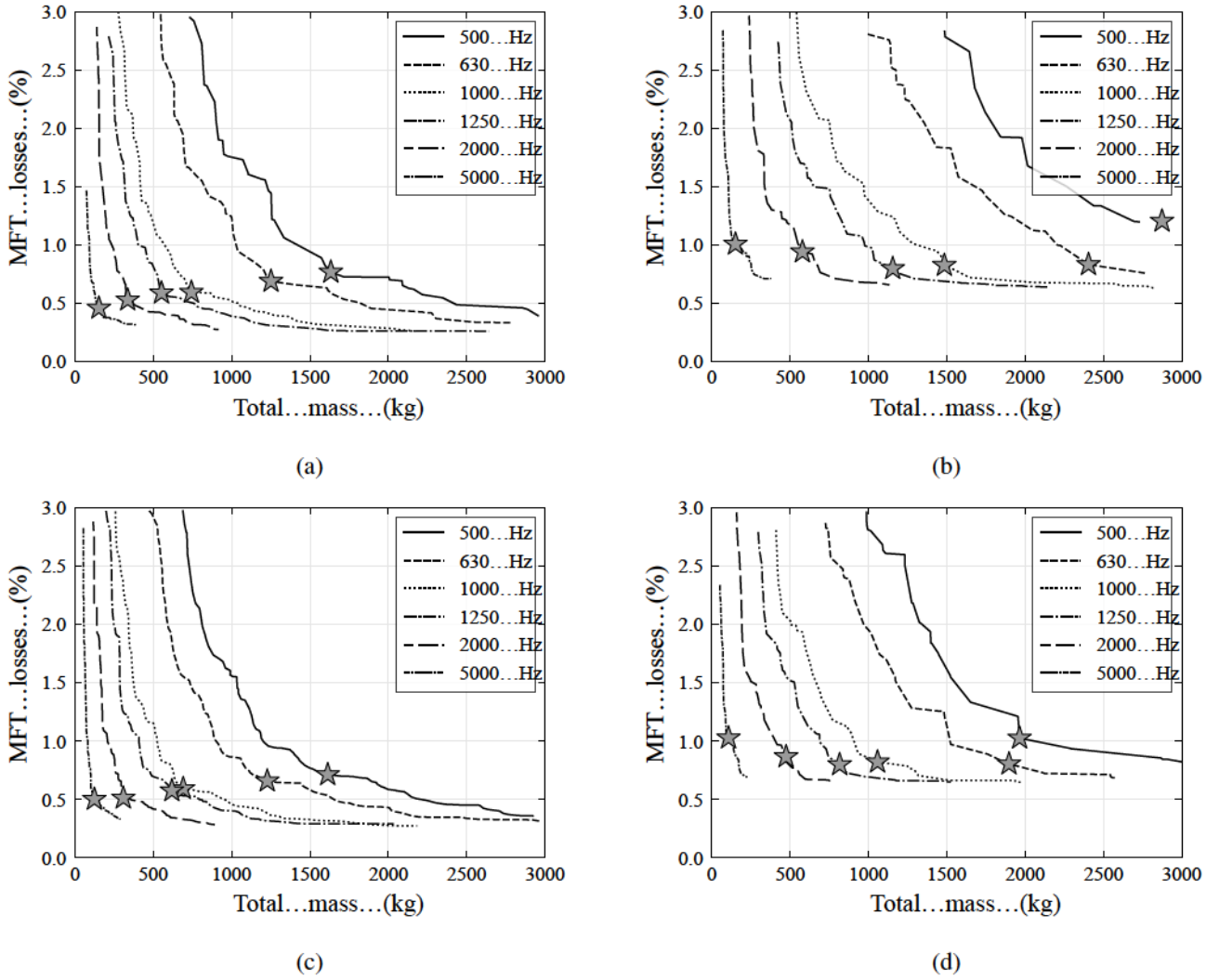

Fig. 6: Results of the transformer optimisation, showing the Pareto-optimal front and selected design for various frequencies for the (a) SAB1, (b) SAB3, (c) DAB1, (d) DAB3

V. Optimisation

The volume, weight, and losses calculations described in the previous sections were carried out for all four converter topologies at frequencies geometrically evenly spaced from 500 Hz to 5 kHz.

A. Transformer optimisation

The results of the transformer optimisation are shown in Fig. 6. The results show that for all topologies, a higher frequency is associated with a reduction in the MFT volume and weight.

The highest frequency of 5 kHz is associated with MFT weights of around 150 kg to 250 kg per module, providing close to a twenty-fold reduction in weight compared to the 500 Hz case. Interestingly, the MFT losses remain relatively constant with frequency and even increase for the lowest tested frequencies. This is due to the reduction in core volume and the mean length of each turn which offset the more frequent core magnetisation and harmonic losses. However, it is important to note that smaller transformer sizes will have more challenges with heat management, which are not taken into consideration here.

The three-phase MFTs, shown in Fig. 6b and Fig. 6d, exhibit both higher losses and mass for the same frequencies compared to their single-phase counterparts, primarily due to the additional core losses and mass from the additional phases. Note that not all the selected designs necessarily fall on the Loss-Mass Pareto-front. This is because the optimisation function also takes into account the transformer volume, which is not shown in the figure.

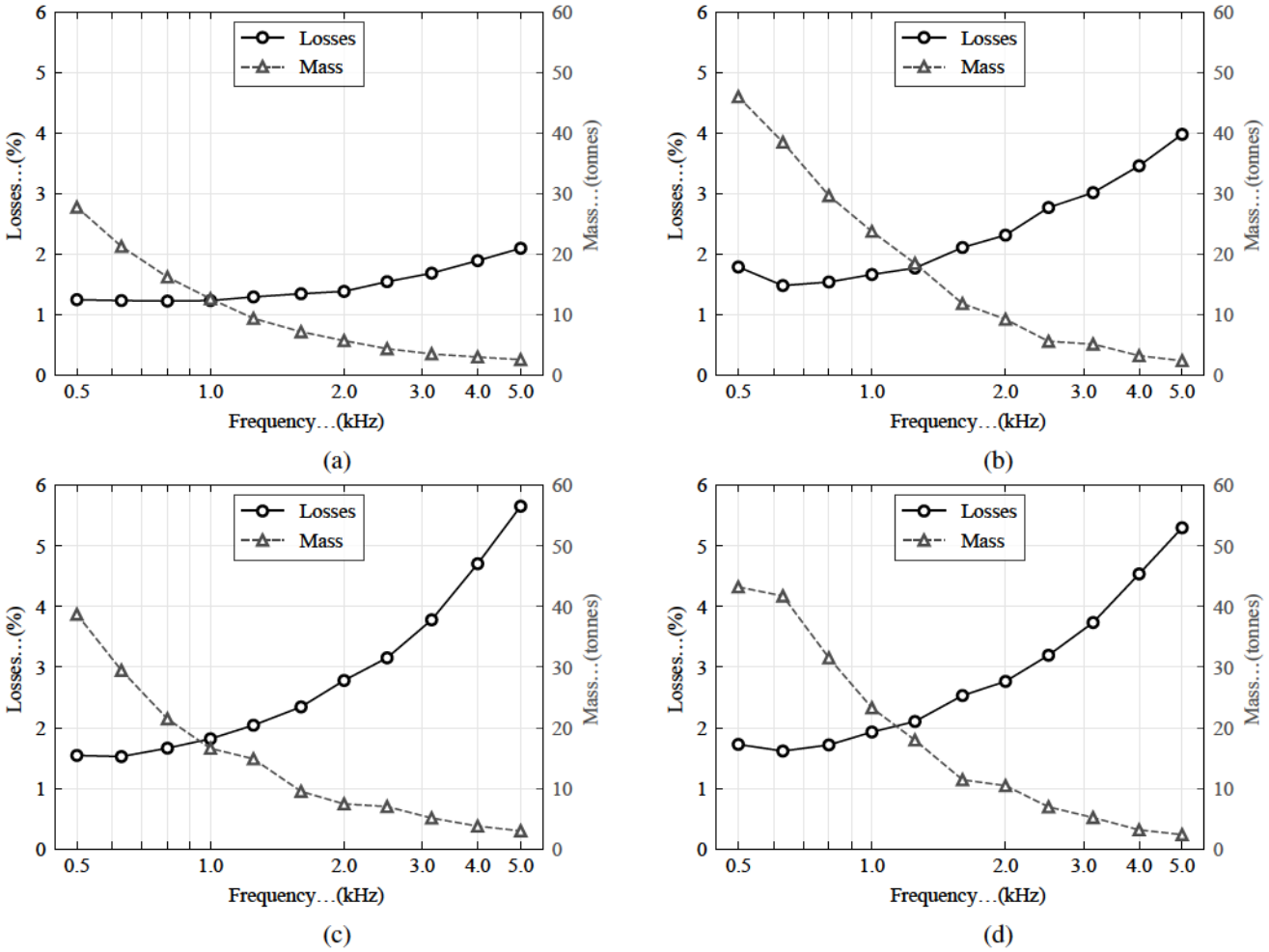

Fig. 7: Results of the converter frequency optimisation, showing the total losses and mass for each converter: (a) SAB1, (b) SAB3, (c) DAB1, (d) DAB3

B. Converter optimisation

The results of the converter frequency optimisation are shown in Fig. 7. The converter losses include both the MFT losses and the representative losses of the semiconductors. It is clear from the figures that for the converters as a whole, there is therefore a trade-off between losses and mass. In practical applications, the specific optimal operating frequency will likely be determined by a range of requirements, beyond just losses and mass. However, a general recommendation can be made based on the marginal gains in power density.

The SAB1 shows the lowest sensitivity to switching frequency, with losses increasing from 1.3% at the lowest frequencies to 2.1% at 5 kHz. The highest marginal gains in power density are made for frequencies up to 2 kHz, reducing the converter mass by 80% for an increase of 0.13% in losses.

The SAB3 results show significantly higher mass and losses at each frequency compared to the SAB1. The higher losses of the SAB3 are primarily due to its inefficient operation at lower outputs, during which it operates in discontinuous current mode, leading to high turn-off losses. Marginal gains in power density for increasing frequencies are high up to a frequency of 1.6 kHz. At this point, the converter mass is approximately 75% lower with 0.3% higher losses compared to the 500 Hz design.

The results for the DAB1 and DAB3 are similar, showing losses that are highly dependent on the converter frequency. For the DAB1, a frequency of 1 kHz provides high power density gains, with a weight reduction of 60% at the cost of a 0.27% increase in losses. For the DAB3, a frequency of 1.25 kHz is required to achieve this 60% weight reduction, leading to an increase of 0.38% in losses compared to the 500 Hz DAB3 design.

VI. Conclusions

This study aimed to determine the optimal operating frequency for DC/DC converters used in future offshore wind turbines that are part of all-DC wind farms. The research considered four topologies, including the SAB1, SAB3, DAB1 and DAB3 converters.

The volume and mass were determined for each converter by analysing a range of MFT designs and selecting an optimal design by performing a multi-objective optimisation aimed at minimising the losses, volume and weight of the MFT. The conduction and switching losses of the semiconductors were calculated using PLECS. This process was performed at frequencies ranging from 500 Hz to 5 kHz.

The resulting optimal operating frequencies for the SAB1, SAB3, DAB1, and DAB3 converters were calculated to be 2 kHz, 1.6 kHz, 1 kHz, and 1.25 kHz, respectively.

References

[1] G. Abeynayake, G. Li, J. Liang, and N. A. Cutululis, "A review on mvdc collection systems for high-power offshore wind farms," in *2019 14th Conference on Industrial and Information Systems (ICIIS)*, pp. 407–412, IEEE, 2019.

[2] V. Timmers, A. Egea-Àlvarez, and A. Gkountaras, "A systematic review of DC wind farm collector cost-effectiveness," in *17th International Conference on AC and DC Power Transmission*, pp. 114–119, IET, 2021.

[3] V. Timmers, A. Egea-Àlvarez, A. Gkountaras, R. Li, and L. Xu, "All-dc offshore wind farms: When are they more cost-effective than ac designs?," *IET Renewable Power Generation*, 2022.

[4] Y. Zhou, D. Macpherson, W. Blewitt, and D. Jovcic, "Comparison of dc-dc converter topologies for offshore wind-farm application," in *6th IET International Conference on Power Electronics, Machines and Drives (PEMD 2012)*, pp. 1–6, IET, 2012.

[5] T. Lagier and P. Ladoux, "A comparison of insulated dc-dc converters for hvdc off-shore wind farms," in *2015 International Conference on Clean Electrical Power (ICCEP)*, pp. 33–39, IEEE, 2015.

[6] M. A. Bahmani, T. Thiringer, A. Rabiei, and T. Abdulahovic, "Comparative study of a multi-mw high-power density dc transformer with an optimized high-frequency magnetics in all-dc offshore wind farm," *IEEE Transactions on power delivery*, vol. 31, no. 2, pp. 857–866, 2015.

[7] R. Barrera-Cardenas and M. Molinas, "Comparative study of wind turbine power converters based on medium-frequency ac-link for offshore dc-grids," *IEEE Journal of Emerging and Selected Topics in Power Electronics*, vol. 3, no. 2, pp. 525–541, 2014.

[8] W. Chen, G. Wang, and X. Zhu, "A family of bidirectional dc/dc converters suitable for asymmetrical power flow requirement," in *2013 IEEE Energy Conversion Congress and Exposition*, pp. 4878–4881, IEEE, 2013.

[9] V. Timmers, A. Egea-Àlvarez, and A. Gkountaras, "Review and comparison of single and dual active bridge converters for MVDC-connected wind turbines," in *21st Wind & Solar Integration Workshop*, 2022.

[10] Y. Sang, A. Junyent-Ferre, and T. C. Green, "Operational principles of three-phase single active bridge dc/dc converters under duty cycle control," *IEEE Trans. Power Electron.*, vol. 35, no. 8, pp. 8737–8750, 2020.

[11] R. W. De Doncker, D. M. Divan, and M. H. Kheraluwala, "A three-phase soft-switched high-power-density DC/DC converter for high-power applications," *IEEE Trans. Ind. Appl.*, vol. 27, no. 1, pp. 63–73, 1991.

[12] Vestas, "V236-15.0 MW." [Online] Available: https://www.vestas.com/en/products/offshore/V236-15MW, 2023. Accessed: 2023-02-21.

[13] Carbon Trust, "Unlocking the next generation of offshore wind: step change to 132kV array systems," tech. rep., Offshore Wind Accelerator, 2022.

[14] M. Mogorovic and D. Dujic, "Sensitivity analysis of medium-frequency transformer designs for solid-state transformers," *IEEE Trans. Power Electron.*, vol. 34, no. 9, pp. 8356–8367, 2018.

[15] G. Abeynayake, G. Li, T. Joseph, J. Liang, and W. Ming, "Reliability and cost-oriented analysis, comparison and selection of multi-level mvdc converters," *IEEE Transactions on Power Delivery*, vol. 36, no. 6, pp. 3945–3955, 2021.

[16] Infineon Technologies AG, "Datasheet FF1800R17IP5." [Online] Available: https://www.infineon.com/cms/en/product/power/igbt/igbt-modules/ff1800r17ip5/, 2020.

[17] Infineon Technologies AG, "Datasheet D471N." [Online] Available: https://www.infineon.com/cms/en/product/power/diodes-thyristors/thyristor-diode-discs/diode-discs/rectifier-diodes/d471n90t/, 2014.

[18] Infineon Technologies AG, "Datasheet FD250R65KE3-K." [Online] Available: https://www.infineon.com/cms/en/product/power/igbt/igbt-modules/fd250r65ke3-k/, 2021.

[19] T. Jimichi, M. Kaymak, and R. W. De Doncker, "Comparison of single-phase and three-phase dual-active bridge dc-dc converters with various semiconductor devices for offshore wind turbines," in *2017 IEEE 3rd International Future Energy Electronics Conference and ECCE Asia (IFEEC 2017-ECCE Asia)*, pp. 591–596, IEEE, 2017.

[20] M. A. Bahmani, T. Thiringer, and M. Kharezy, "Design methodology and optimization of a medium-frequency transformer for high-power DC–DC applications," *IEEE Trans. Ind. Appl.*, vol. 52, no. 5, pp. 4225–4233, 2016.

[21] M. Lambert, F. Sirois, M. Martinez-Duro, and J. Mahseredjian, "Analytical calculation of leakage inductance for low-frequency transformer modeling," *IEEE Transactions on Power Delivery*, vol. 28, no. 1, pp. 507–515, 2012.

[22] L. Max, *Energy evaluation for DC/DC converters in dc-based wind farms*. Lic. thesis, Chalmers University of Technology, 2007.

[23] K. Venkatachalam, C. R. Sullivan, T. Abdallah, and H. Tacca, "Accurate prediction of ferrite core loss with nonsinusoidal waveforms using only steinmetz parameters," in *Proc. IEEE Workshop Comput. Power Electron.*, pp. 36–41, IEEE, 2002.

[24] Plexim GmbH, "PLECS User Manual Version 4.6." [Online] Available: https://www.plexim.com/sites/default/files/plecsmanual.pdf, 2022.